BIOCHEMISTRY
including biophysical chemistry & molecular biology

Article

Oligomers of Parkinson's disease-related alpha-synuclein mutants have similar structures but distinctive membrane permeabilization properties

Anja N.D. Stefanovic, Saskia Lindhoud, Slav A. Semerdzhiev,
Mireille M. A. E. Claessens, and Vinod Subramaniam

Biochemistry, **Just Accepted Manuscript** • DOI: 10.1021/bi501369k • Publication Date (Web): 24 Apr 2015

Just Accepted

Biochemistry is published by the American Chemical Society. 1155 Sixteenth Street N.W., Washington, DC 20036

Oligomers of Parkinson's disease-related alpha-synuclein mutants have similar structures but distinctive membrane permeabilization properties

Anja N. D. Stefanovic[†], *Saskia Lindhoud*[†‡], *Slav A. Semerdzhiev*[†], *Mireille M. A. E. Claessens*[†‡*], *Vinod Subramaniam*[†‡§*]

[†] Nanobiophysics, MESA+ Institute for Nanotechnology, Faculty of Science and Technology University of Twente, PO Box 217, 7500 AE Enschede, The Netherlands,

[‡] MIRA Institute for Biomedical Technology and Technical Medicine, University of Twente, PO Box 217, 7500 AE Enschede, The Netherlands

[§] FOM Institute AMOLF, Science Park 104, 1098 XG Amsterdam, The Netherlands

Corresponding Authors

V. Subramaniam
FOM Institute AMOLF, Science Park 104, 1098 XG Amsterdam, The Netherlands
Tel.: +31 20 7547100 Fax: +31 20 754 7290
Email: subramaniam@amolf.nl

M. M. A. E Claessens
University of Twente, PO Box 217, 7500 AE Enschede, The Netherlands
Tel.:+31 53 489 3157 Fax +31 53 4891105
Email: m.m.a.e.claessens@utwente.nl

ABSTRACT Single amino acid mutations in the human alpha-synuclein (αS) protein are related to early onset Parkinson's disease (PD). In addition to the well-known A30P, A53T, and E46K mutants, recently a number of new familial disease-related αS mutations have been discovered. How these mutations affect the putative physiological function of αS and the disease pathology is still unknown. Here we focus on the H50Q and G51D familial mutants and show that like wild-type αS, H50Q and G51D monomers bind to negatively-charged membranes, form soluble partially-folded oligomers with an aggregation number of ~30 monomers under specific conditions, and can aggregate into amyloid fibrils. We systematically studied the ability of these isolated oligomers to permeabilize membranes composed of anionic phospholipids (DOPG) and membranes mimicking the mitochondrial phospholipid composition (CL:POPE:POPC) using a calcein release assay. SAXS studies on isolated oligomers show that oligomers formed from wild-type αS and the A30P, E46K, H50Q, G51D and A53T disease-related mutants are composed of a similar number of monomers. However, although the binding affinity of the monomeric protein and the aggregation number of the oligomers formed under our specific protocol are comparable for WT αS and H50Q and G51D αS, G51D oligomers cannot disrupt negatively-charged and physiologically-relevant model membranes. Replacement of the membrane-immersed glycine by a negatively charged aspartic acid at position 51 apparently abrogates membrane destabilization, whereas a mutation in the proximal, but solvent exposed part, of the membrane bound alpha helix such as found in the H50Q mutant has little effect on the bilayer disrupting properties of oligomers.

Alpha-synuclein is an intrinsically disordered protein involved in PD.[1, 2] Of all Parkinson's disease patients 10-20% have a hereditary form of the disease. Disease-related mutations include gene duplications, triplications and point mutations in the SNCA gene encoding for αS. In the last 20 years six different SNCA point mutations that result in specific amino acid substitutions in the αS sequence, and that are associated with PD, have been identified: A30P,[3] E46K,[4] H50Q,[5, 6] G51D,[7, 8] A53T,[9] and A53E.[10, 11] Two recently-discovered αS mutations, H50Q and G51D result in rapid progression of the disease.[5-8] The pathology observed in patients with the G51D mutation is further characterized by a moderate response to treatment with levodopa, loss of autonomy, and frequent psychiatric symptoms.[8] The clinical pathology of the H50Q mutation is similar to the disease pathology of the E46K and A53T mutations.[5]

All disease-related amino acid mutations are located in the N-terminal membrane binding part of αS. These mutations may therefore directly affect αS conformation and membrane binding. As observed for wild-type (WT) αS and other disease mutants, G51D and H50Q adopt an α-helical conformation upon binding negatively charged membranes or SDS micelles.[6, 8] The affinity for membranes differs between the WT protein and the known αS mutants; E46K exhibits a higher, A53T similar, and A30P lower binding affinity to negatively charged vesicles than WT αS.[12]

Not only membrane binding but also aggregation into amyloid fibrils is affected by the amino acid substitutions. It was reported that A53T and E46K aggregate faster than WT, while A30P has a slower aggregation rate.[12, 13] In comparison to WT the two newly discovered mutations H50Q and G51D have been reported to show respectively faster and slower kinetics of fibril formation.[6, 8, 14-16]

Studies done in animals, cell systems and model membranes have identified soluble αS oligomers as the potentially toxic species in PD.[17-22] To be able to relate possible toxicity to oligomer structure, αS oligomers have been characterized using various biophysical and biochemical techniques including circular dichroism (CD),[23, 24] single molecule photobleaching,[25] small angle x-ray scattering (SAXS),[1, 26-28] atomic force microscopy (AFM),[29] nuclear magnetic resonance (NMR) spectroscopy,[30] confocal microscopy[31] and electron microscopy.[32] These techniques have shown a variety of shapes and sizes, determined the molecular weight of the oligomers[33, 34] and established the aggregation number of the oligomers, that is, the number of monomers per oligomer.[25, 26, 34]

Here we quantify the membrane binding affinity of the G51D and H50Q mutants, study their aggregation into amyloid fibrils and characterize the aggregation number (that is, the number of monomers per oligomer) and the membrane disrupting properties of oligomers formed from these αS disease mutants. SAXS studies show that oligomers formed from WT and these disease-related mutants are composed of a similar number of monomers. In contrast to the other disease mutants, no differences in G51D membrane binding, fibril formation and oligomer structure compared to WT αS were observed. However, G51D oligomers were not able to permeabilize membranes. We relate the inability of the G51D oligomers to permeabilize negatively charged DOPG and mitochondrial membrane mimics to the position of the amino acid mutation and its role in membrane binding.

MATERIALS AND METHODS

Preparation of oligomeric alpha-synuclein. The expression and purification of human wild-type (WT) and disease-related αS mutants were performed as previously described.[35] Oligomers

from WT and disease-related αS mutants were prepared as described in the literature.[36] The protein concentration was determined by measuring the absorbance using a Shimadzu spectrophotometer at 276 nm, assuming a molar extinction coefficient of 5600 $M^{-1}cm^{-1}$.[37] Oligomers were purified and separated from monomers using size-exclusion chromatography on a SuperdexTM 200 10/300 GL column (GE Healthcare Bio-Sciences AB, Uppsala, Sweden) using 10 mM Tris, 150 mM NaCl, 0.01% NaN_3 as an elution buffer. Separation of oligomers from monomers is based on size, where larger particles (oligomers) elute first. Based on size-exclusion elution profiles oligomer fractions were collected and concentrated up to ~ 100 μM equivalent monomer concentration for SAXS measurements and ~ up to 50 μM equivalent monomer concentration for membrane leakage experiments.

SUVs preparation and binding of αS monomers to SUVs. Small unilamellar vesicles (SUVs) to study membrane binding of monomers using circular dichroism (CD) were prepared using the procedure previously described in Stefanovic *et al*.[36] Although the defects that are typically present in artificial SUVs may affect αS binding, the CD experiments were performed with SUVs instead of LUVs. We made this choice because the scattering of light by LUVs renders the CD spectra very noisy in the information-rich lower wavelength regions. In the literature it has even been suggested that in experiments with LUVs, CD signals obtained below 215 nm need to be discarded.[38] First we used simple negatively charged 1,2-dioleoylphosphatidylglycerol (DOPG) membranes to test the binding of the monomers. However, cell membrane lipid compositions are much more complex. αS colocalizes with mitochondrial membranes[39] and we therefore tested if the binding of αS is comparable between DOPG and mitochondrial membrane mimics (18:1 cardiolipin (CL): 1-palmitoyl, 2-oleoyl phosphatidylethanolamine (POPE): 1-Palmitoyl, 2-oleoyl phosphatidylcholine (POPC) in 4:3:5

ratio). To test the binding affinities of αS for DOPG and CL:POPE:POPC membranes, monomeric WT, G51D and H50Q αS at a concentration of 4 μM were titrated with an SUV solution. Lipid concentrations in the SUV solutions for the titration were between 0.004 and 1.2 mM. The following equation was applied to calculate the binding parameters:[40]

$$R = R_f + (R_0 - R_f)(((-K_d + \sqrt{(K_d^2 + 4CK_d)})/2C)) \quad (1)$$

where R is the measured signal at a given lipid concentration, C is the total lipid concentration, and K_d is the dissociation equilibrium constant. R_f and R_0 are the final and initial signals, respectively. To obtain the K_d values all the data were normalized.

LUV preparation and calcein release assay. Large unilamellar vesicles (LUVs) of DOPG and CL:POPE:POPC for calcein release assays were prepared as previously described.[36] Briefly, the lipid film was hydrated with 50 mM calcein, 10 mM Hepes and 60 mM NaCl to obtain an osmolarity of 320 $mOsm \cdot kg^{-1}$. After subjecting the sample to the 5 freeze-thaw cycles, the solution was extruded 11 times through 100-nm pore size filters (Whatman, Maidstone, UK). Finally, PD-10 columns filled with Sephadex G-100 (GE Healthcare Bio-Sciences AB) were used to remove the free calcein. Calcein release kinetics of the model membranes were followed on a Varian Cary Eclipse fluorometer (Varian Inc., Palo Alto, CA, USA), by recording the emission intensity at 515 nm for excitation at 495 nm. To completely lyse the vesicles Triton X (0.5%) was added. All the data points were normalized using the intensity after Triton X treatment as 100% leakage.

Small-Angle X-ray Scattering. SAXS measurements on αS oligomers were performed in triplicate, i.e. three different batches of each kind of oligomer were made, except for G51D

oligomers, where we only succeeded to get one batch which had enough material. Experiments were performed on samples containing a ~100 μM equivalent monomer concentration of αS dissolved in 10 mM Tris, 150 mM NaCl, 0.01% NaN_3 buffer using the SAXS/WAXS setup at the BM26 - DUBBLE - Dutch-Belgian Beamline, ESRF, Grenoble, France. For G51D oligomers, for two oligomers preparations we could not get sufficiently high concentrations to yield SAXS signals above the limit of detection. Approximately 100 μL of a sample was placed into 1.5 mm quartz capillaries and 2D-images were collected using two Pilatus photon counting detectors. The sample-to-detector distance was 6.6 m. The wavelength for the incident X-ray was 0.1 nm and beam size 2.5×4.5 mm^2 and the energy of the X-rays was 12 eV, resulting in a q-range of ~0.03-1.5 nm^{-1}. For data reduction, buffer (background) scattering values were subtracted from the protein solution scattering values and standards were used to convert the scattering values to values on an absolute scale.

First we determined the radius of gyration, R_g and $I(0)$, using Guinier's law: $I(q) = I(0)exp\left(-q^2 R_g^2/3\right)$. Guinier plots provide information about the average size of the particles in the solution. The oligomers studied are in the first approximation spherical structures. For spherical particles, Guinier plots, where $(ln(I(q))$ is plotted as a function of q^2, give a linear dependency for $qR_g < 1.3$. From the slope of this curve R_g was determined at $qR_g < 1.3$ and $I(0)$ was obtained by extrapolation to $q = 0$.

The aggregation numbers of the oligomers can be determined indirectly by an equation that describes the scattering of the particles in a solution:

$$I(q) = nV^2 \Delta\rho_{rel.sol}{}^2 P(q) S(q) \qquad (2)$$

where n is the number of scattering particles per unit volume, V is the volume of the particle, and $\Delta\rho_{rel.sol} = \rho_{particle} - \rho_{solvent}$ is the excess scattering length density or contrast, $P(q)$ is the form factor of the particle and is related to the particle's shape, $S(q)$ is the structure factor that defines inter-particle interactions in the solution.

When the SAXS intensities are extrapolated to $q = 0$, then $I(0)$ is given by[41]

$$I(0) = nV^2\Delta\rho_{rel.sol}{}^2 \quad (3)$$

In our case $\Delta\rho_{rel.sol}$ was calculated to be 0.0002864 nm^{-2} using contrast calculator in the SAXS utilities program (extension of Matlab),[42] using $\rho_{particle} = 1.37\ g/cm^3$ as the experimentally determined average protein density.[43, 44] $I(0)$ and the volume V can be calculated using the R_g determined via the Guinier approximation. For calculating the molecular weight, M_w, of the particles/proteins, the following equation was applied:[45]

$$I(0) = N(\Delta\rho V)^2 = c\Delta\rho^2 v^2 M_w / N_A \quad (4)$$

where N_A is Avogadro's number and c is the protein or particle concentration. The aggregation number N is extracted by dividing the M_w estimated from equation 4 by the molecular weight of the αS monomer. To visualize if disordered regions are present in the oligomer the data obtained are also presented in a Kratky plot by plotting $I(q)q^2$ *versus* q.[46]

Kinetics of aggregation. Solutions containing 100 μM αS monomers of the different disease mutants in 10 mM Tris-HCl, 100 mM NaCl, pH 7.4 were incubated at 37°C under constant shaking in a Tecan SAFIRE II plate reader. Protein aggregation into amyloid fibrils was followed in a Thioflavin T (ThT) fluorescence assay. For this purpose 5 μM ThT was used.

Changes in ThT fluorescence were followed using an excitation wavelength of 446 nm and bandwidth 10 nm and the emission intensity at 485 nm was recorded with emission bandwidth of 10 nm as a function of time. Aggregation lag times were determined as previously described by Willander et al.[47]

Atomic force microscopy (AFM). To visualize the amyloid fibrils, samples were prepared for AFM imaging. Samples of aggregated protein (after ThT assay) were placed on the mica substrate using the procedure described by Sweers *et al*.[48] The dried samples were visualized by AFM using tapping mode. During these experiments an NSC 36 tip B was used, with a force constant of 1.75 N/m (NanoAndMore GmbH, Wetzlar, Germany). All images obtained during these experiments are 4 x 4 μm in size, 512 pixels with a z-range of 20 nm.

RESULTS

Binding of αS monomers to SUVs. To determine the membrane binding affinities of WT, H50Q and G51D αS to SUVs composed of DOPG and CL:POPE:POPC, we titrated αS monomers with different concentrations of SUVs. Conformational changes of WT, G51D and H50Q αS monomers upon binding to the membranes were followed by recording CD spectra between 190 and 260 nm. Representative CD spectra of the titration of WT monomers with DOPG and CL:POPE:POPC SUVs are given in Supporting Information **Figure S1**. To follow α-helix formation and hence membrane binding, the mean residue ellipticities (MRE) at 222 nm are presented as a function of the lipid concentration in **Figure 1**. As described in the Materials and Methods section, a simple binding model was used to calculate the equilibrium dissociation constant K_d from the titration of αS monomers with DOPG (Figure 1A) and CL:POPE:POPC (Figure 1B). The dissociation constants obtained by fitting the titration curves for lipid mixtures

and WT, G51D and H50Q αS are given in **Table 1**. For all three αS species the K_d values were of the same order of magnitude, but the affinity for DOPG membranes was an order of magnitude higher than the affinity for the CL:POPE:POPC mitochondrial membrane mimics. The observed higher affinity for DOPG membranes is in agreement with previous studies on membrane binding of WT and the A30P, A53T, and E46K amino acid mutations in αS.[24, 49, 50]

Aggregation studies. To further characterize the disease-related αS mutants the aggregation of 100 μM monomers into amyloid fibrils was studied in 10 mM Tris-HCl buffer, 100 mM NaCl, pH 7.4. At these buffer conditions the aggregation lag times of most disease mutants were comparable to the lag time observed for WT protein, with only A30P exhibiting significant differences (Figure 2A). The aggregation lag time of A30P was more than two-fold longer than the lag time for the other proteins. The fibrils that were obtained with the different disease mutants were visualized using AFM. This analysis confirmed that all disease mutants are able to form amyloid fibrils. The morphologies of the amyloid fibrils formed by WT and the disease-related mutants are qualitatively comparable (Figure 2B).

Calcein release assay. The toxicity of αS aggregation in PD has been related to oligomeric species that bind and permeabilize membranes. We performed a calcein release assay to test the ability of oligomers of disease-related αS mutants to permeabilize membranes composed of anionic phospholipids (DOPG) and membranes mimicking the mitochondrial phospholipid composition (CL:POPE:POPC). LUVs were filled with calcein at a self-quenching concentration; upon incubation with oligomers an increase of fluorescence emission intensity results from dye dilution due to membrane permeabilization. When oligomers were added, they induced fast calcein leakage from DOPG LUVs which was not observed for LUVs in which the mitochondrial membrane composition was mimicked. In Figure 3 the normalized leakage (%)

measured 30 minutes after incubation with the respective oligomeric species is represented as a function of oligomer concentration (monomer equivalent). Except for G51D, all oligomers were able to induce almost complete permeabilization of negatively charged DOPG membranes at the highest concentrations tested. The disease-related oligomers are slightly more efficient than WT oligomers in permeabilizing membranes; lower concentrations are required for comparable leakage (Figure 3A). Oligomer-induced calcein leakage from LUVs composed of CL:POPE:POPC was very slow. Dye leakage reached a plateau approximately 18 hours after oligomer addition.[36] G51D and E46K oligomers were not able to induce leakage from the CL:POPE:POPC LUVs (Figure 3B). Even for the A53T and A30P oligomers that were most efficient in permeabilizing LUVs of this membrane composition, the maximum leakage only reached 30%.

Aggregation number. Although the membrane binding affinity and aggregation kinetics of G51D, H50Q and WT αS monomers are comparable, the ability of oligomers formed from these variants to permeabilize membranes differs. Although these proteins display similar membrane-binding affinity for the monomers, the different permeabilization propensity of the oligomers may result from differences in oligomer composition and structure. The aggregation numbers of the oligomers were therefore characterized by SAXS. Figure 4A shows the scattering curves for the oligomers of WT αS and five different disease mutants. The scattering curves look very similar in shape. From these scattering curves the aggregation numbers of the oligomers were estimated using the following procedure: The R_g and $I(0)$ were determined using the Guinier approximation (Figure 4B). To calculate the aggregation number, the molecular weight (M_w) of protein oligomers has to be determined.[51, 52] We used equations 2 and 3 to determine the aggregation numbers. The values for R_g and $I(0)$ determined from the Guinier approximation,

and the aggregation numbers derived for the different oligomers can be found in **Figure 4C** and **Table 2**.

As we can observe in **Figure 4C** the aggregation number (number of monomers per oligomer, $N_{m/1oli}$) estimated for the oligomers of each disease-related mutant was approximately 30 which agrees well with previously published data from our group on WT oligomers and dopamine-induced oligomers using a single molecule photobleaching approach.[25, 53] This value is also consistent with those found by Otzen and coworkers using SAXS.[34]

We further analyzed the data by plotting $q^2I(q)$ versus q in Kratky plots. These Kratky plots are used to monitor the degree of the compactness of a protein in order to evaluate the extent of folding of proteins. Globular molecules follow Porod's law resulting in a bell-shaped curve, whereas extended molecules, such as unfolded peptides, have a plateau or increase at higher q-ranges.[54] The Kratky plots presented in **Figure 5** and Supporting Information **Figure S2** show part of a bell shaped curve and increase of q^2I with increasing q which indicates that oligomers composed of WT and disease-related αS mutants are composed of partially folded proteins.

DISCUSSION

The H50Q and G51D disease mutants have been reported to adopt an α-helical conformation when binding membranes.[6, 8] Here we have determined the binding affinities of monomeric WT, G51D and H50Q to vesicles composed of negatively charged DOPG and a phospholipid composition mimicking the mitochondrial membrane. Our CD data show that WT, G51D and H50Q have comparable binding affinities to negatively charged DOPG membranes, while small differences between the mutants were visible on CL:POPE:POPC vesicles. In the latter case, an approximately 4 times higher binding affinity was observed for WT compared to H50Q. The

membrane composition had a large effect on the observed K_d; αS has an order of magnitude higher affinity for DOPG than for CL:POPE:POPC membranes. It is known that a single amino-acid substitution can cause changes in binding affinity, with A30P monomers demonstrating a lower binding affinity than E46K, A53T and WT.[12] Whether and how αS amino-acid mutations affect membrane binding most likely depends on the position of the amino-acid substitution. However, although in G51D a membrane-immersed residue is replaced with an acidic amino acid, this change has only a small effect on K_d. The lack of a profound effect of the G51D point mutation on LUV binding may result from its proximity to the postulated break in the membrane bound α-helix.[55] The replacement of H by Q in the H50Q mutation involves only a small change in the polarity of a solvent-exposed residue and has probably therefore little effect on membrane binding.

Under the conditions studied here, all the disease mutants form amyloid fibrils and only for A30P was the aggregation lag time significantly increased compared to WT and the other disease mutants (see **Figure 2A and Figure S2**). The shape of the aggregation profiles looks similar for all the mutants, suggesting that the fibril growth mechanism is comparable (**Figure 2A**). The morphologies of the fibrils in solution after a ThT aggregation experiment were studied by AFM, which confirmed that all mutants form qualitatively similar fibrils. Although it was previously reported that H50Q aggregated faster and G51D slower than WT,[6, 8, 14, 15] we did not observe any significant difference in aggregation kinetics between these disease mutants and WT αS. This difference could be caused by the experimental conditions used; both the buffer and αS concentrations used in our experiments were different from the published reports. Whereas we studied the aggregation of 100 μM αS monomers in 10 mM Tris, 100 mM NaCl, pH 7.4, Ghosh et al.[6] used 3 times higher H50Q concentration in 20 mM Glycine-NaOH buffer, and reported a

difference in aggregation kinetics between H50Q and WT. The slower aggregation kinetics of G51D compared to WT[8] was observed in 20 mM Tris, 150 mM KCl, pH 7.5 which is similar to our aggregation conditions.

A growing consensus suggests that oligomers are the toxic species involved in PD.[29, 56] Oligomers are thought to disrupt the integrity of cellular membranes. Here we tested if oligomers of the different αS disease mutants differ in their ability to induce membrane permeabilization. Our results showed a large difference in the permeabilization of DOPG membranes by G51D oligomers compared to the other oligomers. G51D oligomers could not induce more than 20% permeabilization of DOPG membranes. Oligomers of the newly discovered H50Q mutant showed similar permeabilization of DOPG vesicles as WT oligomers. However oligomers of both newly discovered mutants are less prone to induce permeabilization of mitochondrial model membranes than WT, where G51D oligomers showed almost no permeabilization (**Figure 3**).

WT, G51D and H51Q monomers do not differ much in membrane affinity (**Figure 1**). The differences in the ability of αS oligomers to permeabilize membranes may therefore be related to differences in oligomer structure. SAXS has proven to be a very useful technique to obtain more detailed insights on the structure and size of protein oligomers.[27, 34] We therefore performed SAXS investigations of oligomers formed from WT and a range of disease-related point mutants.

However, our data show that the size and aggregation number of the 6 different αS oligomers studied are very similar. All oligomers studied yield aggregation numbers ~ 30 (**Figure 4C**), and the Kratky plots show that all oligomers are partially folded structures (**Figure 5 and Figure S2**). CD measurements confirm the partially folded nature of the oligomer and show that oligomers contain β-sheets.[23, 36] The partially folded nature of the oligomer is also in good

agreement with tryptophan quenching experiments which suggest that residues 4-90 make up the core of the WT oligomer while the C-terminus remains solvent exposed.[57] The similarities in aggregation number and structure observed by SAXS can however not exclude that differences exist. SAXS probes the average size of the species in solution and it is very difficult to distinguish between 2 or 3 different species. The mean aggregation number we derive for this WT oligomer is comparable to the values found with SAXS[34] by other investigators, and with single molecule photobleaching experiments.[25] The difference in permeabilization cannot therefore be attributed to the oligomer aggregation number and overall structure.

Although the binding affinity of WT and G51D monomers are comparable, the exchange of a small neutral amino acid G with polar negatively-charged D resulted in lower oligomer-induced permeabilization of DOPG membranes. The comparable binding affinity indicates that the G51D substitution does not result in large changes in the membrane binding α-helical structure of the monomer. Lashuel and coworkers have shown that G51D monomers show qualitatively similar binding profiles to WT protein, but have also suggested that residues 45-55 in the G51D mutant exhibit somewhat decreased helicity, which may be attributed to N-terminal fraying of helix 2 in the presence of the glycine to aspartic acid mutation.[16] In studies with acidic vesicles, these authors have also shown that, consistent with our studies, the inherent capacity of helix formation by the G51D mutant is not abrogated, but that the mutation interferes specifically with negatively charged membranes. These changes in biochemical properties of the G51D mutant are likely also manifested in the G51D oligomer.

We note that with the G51D substitution an acidic amino acid (D) would become exposed to a lipophilic environment.[55] Although the G51D αS oligomers bind membranes, the partially folded structure of the oligomer may prevent binding of the complete α-helix. In the absence of a high-

resolution structure in the membrane-bound state, we speculate that when fewer residues per monomer are available, the relative contribution of position 51 may become more important. Thus, the G51D oligomer may either not bind membranes effectively or the G51D substitution may make it more difficult to distort the lipid bilayer because fewer amino acid residues are immersed in the bilayer.

ASSOCIATED CONTENT

Supporting Information

CD spectra of the titration of WT αS with DOPG SUVS and three-dimensional composite of Kratky plots shown in Figure 5 are presented in the SI. This material is available free of charge via the Internet at http://pubs.acs.org

AUTHOR INFORMATION

Author Contributions

The manuscript was written through contributions of all authors.

Funding Sources

This work was financially supported by the "Nederlandse Organisatie voor Wetenschappelijk Onderzoek" (NWO) through the NWO-CW TOP program number 700.58.302 to VS. Additional funding was provided by Stichting International Parkinson Fonds. For SAXS experiments performed in ESRF, Grenoble, funding was provided by an NWO grant to SL under program number 195.068.739 for beam time (beam time number 26-02-664). SL acknowledges funding by an NWO VENI award, grant number 722.013.013. VS also acknowledges support from the Foundation for Fundamental Research on Matter (FOM), which is part of the Netherlands

Organisation for Scientific Research (NWO) in the context of the FOM program "A Single Molecule View on Protein Aggregation".

ACKNOWLEDGMENT

We thank Kirsten van Leijenhorst-Groener and Nathalie Schilderink for assistance in expression and purification of alpha-synuclein. SAXS experiments were performed in ESRF, Grenoble, France on the SAXS/WAXS configuration of BM26B (DUBBLE) experiment number 26-02-664. We thank Dr G. Portale (Beamline Scientist) for the help in performing SAXS experiments.

ABBREVIATIONS

αS, alpha-synuclein; AFM, atomic force microscope; CD, circular dichroism; CL, 18:1 cardiolipin; DOPG, 1,2-dioleoylphosphatidylglycerol; LUV, large unilamellar vesicle MRE mean residue ellipticities; PD, Parkinson's disease; POPC, 1-Palmitoyl, 2-oleoyl phosphatidylcholine; POPE, 1-palmitoyl, 2-oleoyl phosphatidylethanolamine; SAXS, small angle X-ray scattering; SUV, small unilamellar vesicle; WT, wild type.

REFERENCES

1. Breydo, L., Wu, J. W., and Uversky, V. N. (2012) Alpha-synuclein misfolding and Parkinson's disease, *Biochim. Biophys. Acta 1822*, 261-285.
2. Uversky, V. N., Lee, H. J., Li, J., Fink, A. L., and Lee, S. J. (2001) Stabilization of partially folded conformation during alpha-synuclein oligomerization in both purified and cytosolic preparations, *J. Biol. Chem. 276*, 43495-43498.
3. Kruger, R., Kuhn, W., Muller, T., Woitalla, D., Graeber, M., Kosel, S., Przuntek, H., Epplen, J. T., Schols, L., and Riess, O. (1998) Ala30Pro mutation in the gene encoding alpha-synuclein in Parkinson's disease, *Nat. Genet. 18*, 106-108.
4. Zarranz, J. J., Alegre, J., Gomez-Esteban, J. C., Lezcano, E., Ros, R., Ampuero, I., Vidal, L., Hoenicka, J., Rodriguez, O., Atares, B., Llorens, V., Gomez Tortosa, E., del Ser, T., Munoz, D. G., and de Yebenes, J. G. (2004) The new mutation, E46K, of alpha-synuclein causes Parkinson and Lewy body dementia, *Ann. Neurol. 55*, 164-173.
5. Appel-Cresswell, S., Vilarino-Guell, C., Encarnacion, M., Sherman, H., Yu, I., Shah, B., Weir, D., Thompson, C., Szu-Tu, C., Trinh, J., Aasly, J. O., Rajput, A., Rajput, A. H., Jon

Stoessl, A., and Farrer, M. J. (2013) Alpha-synuclein p.H50Q, a novel pathogenic mutation for Parkinson's disease, *Mov. Disord. 28*, 811-813.

6. Ghosh, D., Mondal, M., Mohite, G. M., Singh, P. K., Ranjan, P., Anoop, A., Ghosh, S., Jha, N. N., Kumar, A., and Maji, S. K. (2013) The Parkinson's Disease-Associated H50Q Mutation Accelerates alpha-Synuclein Aggregation in Vitro, *Biochemistry 52*, 6925-6927.
7. Kiely, A. P., Asi, Y. T., Kara, E., Limousin, P., Ling, H., Lewis, P., Proukakis, C., Quinn, N., Lees, A. J., Hardy, J., Revesz, T., Houlden, H., and Holton, J. L. (2013) alpha-Synucleinopathy associated with G51D SNCA mutation: a link between Parkinson's disease and multiple system atrophy?, *Acta Neuropathol. 125*, 753-769.
8. Lesage, S., Anheim, M., Letournel, F., Bousset, L., Honore, A., Rozas, N., Pieri, L., Madiona, K., Durr, A., Melki, R., Verny, C., Brice, A., and French Parkinson's Disease Genetics Study, G. (2013) G51D alpha-synuclein mutation causes a novel parkinsonian-pyramidal syndrome, *Ann. Neurol. 73*, 459-471.
9. Polymeropoulos, M. H., Lavedan, C., Leroy, E., Ide, S. E., Dehejia, A., Dutra, A., Pike, B., Root, H., Rubenstein, J., Boyer, R., Stenroos, E. S., Chandrasekharappa, S., Athanassiadou, A., Papapetropoulos, T., Johnson, W. G., Lazzarini, A. M., Duvoisin, R. C., Di Iorio, G., Golbe, L. I., and Nussbaum, R. L. (1997) Mutation in the alpha-synuclein gene identified in families with Parkinson's disease, *Science 276*, 2045-2047.
10. Pasanen, P., Myllykangas, L., Siitonen, M., Raunio, A., Kaakkola, S., Lyytinen, J., Tienari, P. J., Pöyhönen, M., and Paetau, A. (2014) A novel α-synuclein mutation A53E associated with atypical multiple system atrophy and Parkinson's disease-type pathology, *Neurobiol. Aging 35*, 2180.e2181-2180.e2185.
11. Ghosh, D., Sahay, S., Ranjan, P., Salot, S., Mohite, G. M., Singh, P. K., Dwivedi, S., Carvalho, E., Banerjee, R., Kumar, A., and Maji, S. K. (2014) The Newly Discovered Parkinson's Disease Associated Finnish Mutation (A53E) Attenuates alpha-Synuclein Aggregation and Membrane Binding, *Biochemistry 53*, 6419-6421.
12. Choi, W., Zibaee, S., Jakes, R., Serpell, L. C., Davletov, B., Crowther, R. A., and Goedert, M. (2004) Mutation E46K increases phospholipid binding and assembly into filaments of human alpha-synuclein, *FEBS Lett. 576*, 363-368.
13. Lemkau, L. R., Comellas, G., Kloepper, K. D., Woods, W. S., George, J. M., and Rienstra, C. M. (2012) Mutant protein A30P alpha-synuclein adopts wild-type fibril structure, despite slower fibrillation kinetics, *J. Biol. Chem. 287*, 11526-11532.
14. Khalaf, O., Fauvet, B., Oueslati, A., Dikiy, I., Mahul-Mellier, A.-L., Ruggeri, F. S., Mbefo, M., Vercruysse, F., Dietler, G., Lee, S.-J., Eliezer, D., and Lashuel, H. A. (2014) The H50Q mutation enhances α-synuclein aggregation, secretion and toxicity, *J. Biol. Chem. 289*, 21856-21876.
15. Rutherford, N. J., Moore, B. D., Golde, T. E., and Giasson, B. I. (2014) Divergent effects of the H50Q and G51D SNCA mutations on the aggregation of alpha-synuclein, *J. Neurochem. 131,* 859-867.
16. Fares, M. B., Ait-Bouziad, N., Dikiy, I., Mbefo, M. K., Jovicic, A., Kiely, A., Holton, J. L., Lee, S. J., Gitler, A. D., Eliezer, D., and Lashuel, H. A. (2014) The novel Parkinson's disease linked mutation G51D attenuates in vitro aggregation and membrane binding of alpha-synuclein, and enhances its secretion and nuclear localization in cells, *Hum. Mol. Genet. 23,* 4491-4509.

17. Fredenburg, R. A., Rospigliosi, C., Meray, R. K., Kessler, J. C., Lashuel, H. A., Eliezer, D., and Lansbury, P. T. (2007) The Impact of the E46K Mutation on the Properties of α-Synuclein in Its Monomeric and Oligomeric States, *Biochemistry 46*, 7107-7118.
18. Xilouri, M., Vogiatzi, T., Vekrellis, K., Park, D., and Stefanis, L. (2009) Abberant α-Synuclein Confers Toxicity to Neurons in Part through Inhibition of Chaperone-Mediated Autophagy, *PLoS One 4*, e5515.
19. Cuervo, A. M., Stefanis, L., Fredenburg, R., Lansbury, P. T., and Sulzer, D. (2004) Impaired degradation of mutant alpha-synuclein by chaperone-mediated autophagy, *Science 305*, 1292-1295.
20. Gureviciene, I., Gurevicius, K., and Tanila, H. (2007) Role of alpha-synuclein in synaptic glutamate release, *Neurobiol. Dis. 28*, 83-89.
21. Dimant, H., Kalia, S. K., Kalia, L. V., Zhu, L. N., Kibuuka, L., Ebrahimi-Fakhari, D., McFarland, N. R., Fan, Z., Hyman, B. T., and McLean, P. J. (2013) Direct detection of alpha synuclein oligomers in vivo, *Acta Neuropathol Commun 1*, 6.
22. Winner, B., Jappelli, R., Maji, S., Desplats, P., Boyer, L., Aigner, S., Hetzer, C., Loher, T., Vilar, M., and Campioni, S. (2011) In vivo demonstration that alpha-synuclein oligomers are toxic, *Proc. Natl. Acad. Sci. U. S. A. 108*, 4194 - 4199.
23. van Rooijen, B. D., Claessens, M. M., and Subramaniam, V. (2009) Lipid bilayer disruption by oligomeric alpha-synuclein depends on bilayer charge and accessibility of the hydrophobic core, *Biochim. Biophys. Acta 1788*, 1271-1278.
24. Davidson, W. S., Jonas, A., Clayton, D. F., and George, J. M. (1998) Stabilization of alpha-synuclein secondary structure upon binding to synthetic membranes, *J. Biol. Chem. 273*, 9443-9449.
25. Zijlstra, N., Blum, C., Segers-Nolten, I. M., Claessens, M. M., and Subramaniam, V. (2012) Molecular composition of sub-stoichiometrically labeled alpha-synuclein oligomers determined by single-molecule photobleaching, *Angew. Chem. Int. Ed. Engl. 51*, 8821-8824.
26. Giehm, L., Svergun, D. I., Otzen, D. E., and Vestergaard, B. (2011) Low-resolution structure of a vesicle disrupting α-synuclein oligomer that accumulates during fibrillation, *Proc. Natl. Acad. Sci. U. S. A. 108*, 3246-3251.
27. Pham, C. L., Kirby, N., Wood, K., Ryan, T., Roberts, B., Sokolova, A., Barnham, K. J., Masters, C. L., Knott, R. B., Cappai, R., Curtain, C. C., and Rekas, A. (2014) Guanidine hydrochloride denaturation of dopamine-induced alpha-synuclein oligomers: a small-angle X-ray scattering study, *Proteins 82*, 10-21.
28. Lorenzen, N., Lemminger, L., Pedersen, J. N., Nielsen, S. B., and Otzen, D. E. (2014) The N-terminus of alpha-synuclein is essential for both monomeric and oligomeric interactions with membranes, *FEBS Lett. 588*, 497-502.
29. Danzer, K. M., Haasen, D., Karow, A. R., Moussaud, S., Habeck, M., Giese, A., Kretzschmar, H., Hengerer, B., and Kostka, M. (2007) Different species of alpha-synuclein oligomers induce calcium influx and seeding, *J. Neurosci. 27*, 9220-9232.
30. Bodner, C. R., Maltsev, A. S., Dobson, C. M., and Bax, A. (2010) Differential phospholipid binding of alpha-synuclein variants implicated in Parkinson's disease revealed by solution NMR spectroscopy, *Biochemistry 49*, 862-871.
31. van Rooijen, B. D., Claessens, M. M., and Subramaniam, V. (2008) Membrane binding of oligomeric alpha-synuclein depends on bilayer charge and packing, *FEBS Lett. 582*, 3788-3792.

32. Lashuel, H. A., Petre, B. M., Wall, J., Simon, M., Nowak, R. J., Walz, T., and Lansbury, P. T. (2002) α-Synuclein, Especially the Parkinson's Disease-associated Mutants, Forms Pore-like Annular and Tubular Protofibrils, *J. Mol. Biol. 322*, 1089-1102.
33. Rekas, A., Knott, R., Sokolova, A., Barnham, K., Perez, K., Masters, C., Drew, S., Cappai, R., Curtain, C., and Pham, C. L. (2010) The structure of dopamine induced α-synuclein oligomers, *Eur. Biophys. J. 39*, 1407-1419.
34. Lorenzen, N., Nielsen, S. B., Buell, A. K., Kaspersen, J. D., Arosio, P., Vad, B. S., Paslawski, W., Christiansen, G., Valnickova-Hansen, Z., Andreasen, M., Enghild, J. J., Pedersen, J. S., Dobson, C. M., Knowles, T. P., and Otzen, D. E. (2014) The role of stable alpha-synuclein oligomers in the molecular events underlying amyloid formation, *J. Am. Chem. Soc. 136*, 3859-3868.
35. Sidhu, A., Segers-Nolten, I., and Subramaniam, V. (2014) Solution conditions define morphological homogeneity of alpha-synuclein fibrils, *Biochim. Biophys. Acta 1844*, 2127-2134.
36. Stefanovic, A. N., Stockl, M. T., Claessens, M. M., and Subramaniam, V. (2014) alpha-Synuclein oligomers distinctively permeabilize complex model membranes, *FEBS J. 281*, 2838-2850.
37. Pace, C. N., Vajdos, F., Fee, L., Grimsley, G., and Gray, T. (1995) How to measure and predict the molar absorption coefficient of a protein, *Protein Sci. 4*, 2411-2423.
38. Ladokhin, A. S., Fernandez-Vidal, M., and White, S. H. (2010) CD spectroscopy of peptides and proteins bound to large unilamellar vesicles, *J. Membr. Biol. 236*, 247-253.
39. Devi, L., Raghavendran, V., Prabhu, B. M., Avadhani, N. G., and Anandatheerthavarada, H. K. (2008) Mitochondrial import and accumulation of alpha-synuclein impair complex I in human dopaminergic neuronal cultures and Parkinson disease brain, *J. Biol. Chem. 283*, 9089-9100.
40. Honda, S., Kobayashi, N., Munekata, E., and Uedaira, H. (1999) Fragment reconstitution of a small protein: folding energetics of the reconstituted immunoglobulin binding domain B1 of streptococcal protein G, *Biochemistry 38*, 1203-1213.
41. Fisher, C. K., and Stultz, C. M. (2011) Constructing ensembles for intrinsically disordered proteins, *Curr. Opin. Struct. Biol. 21*, 426-431.
42. Sztucki, M., and Narayanan, T. (2007) Development of an ultra-small-angle X-ray scattering instrument for probing the microstructure and the dynamics of soft matter, *J. Appl. Crystallogr. 40*, s459-s462.
43. Gekko, K., and Noguchi, H. (1979) Compressibility of globular proteins in water at 25.degree.C, *J. Phys. Chem. 83*, 2706-2714.
44. Fischer, H., Polikarpov, I., and Craievich, A. F. (2004) Average protein density is a molecular-weight-dependent function, *Protein science : a publication of the Protein Society 13*, 2825-2828.
45. Jacques, D. A., and Trewhella, J. (2010) Small-angle scattering for structural biology--expanding the frontier while avoiding the pitfalls, *Protein Sci. 19*, 642-657.
46. Doniach, S. (2001) Changes in biomolecular conformation seen by small angle X-ray scattering, *Chem. Rev. 101*, 1763-1778.
47. Willander, H., Presto, J., Askarieh, G., Biverstal, H., Frohm, B., Knight, S. D., Johansson, J., and Linse, S. (2012) BRICHOS domains efficiently delay fibrillation of amyloid beta-peptide, *J. Biol. Chem. 287*, 31608-31617.

48. Sweers, K., van der Werf, K., Bennink, M., and Subramaniam, V. (2011) Nanomechanical properties of alpha-synuclein amyloid fibrils: a comparative study by nanoindentation, harmonic force microscopy, and Peakforce QNM, *Nanoscale Res Lett 6*, 270.
49. Shvadchak, V. V., Falomir-Lockhart, L. J., Yushchenko, D. A., and Jovin, T. M. (2011) Specificity and kinetics of alpha-synuclein binding to model membranes determined with fluorescent excited state intramolecular proton transfer (ESIPT) probe, *J. Biol. Chem. 286*, 13023-13032.
50. Shvadchak, V. V., Yushchenko, D. A., Pievo, R., and Jovin, T. M. (2011) The mode of alpha-synuclein binding to membranes depends on lipid composition and lipid to protein ratio, *FEBS Lett. 585*, 3513-3519.
51. Fischer, H., de Oliveira Neto, M., Napolitano, H. B., Polikarpov, I., and Craievich, A. F. (2010) Determination of the molecular weight of proteins in solution from a single small-angle X-ray scattering measurement on a relative scale, *J Appl Cryst 43*, 101-109.
52. Bernado, P., and Svergun, D. I. (2012) Structural analysis of intrinsically disordered proteins by small-angle X-ray scattering, *Molecular bioSystems 8*, 151-167.
53. Zijlstra, N., Claessens, Mireille M. A. E., Blum, C., and Subramaniam, V. (2014) Elucidating the Aggregation Number of Dopamine-Induced α-Synuclein Oligomeric Assemblies, *Biophys. J. 106*, 440-446.
54. Putnam, C. D., Hammel, M., Hura, G. L., and Tainer, J. A. (2007) X-ray solution scattering (SAXS) combined with crystallography and computation: defining accurate macromolecular structures, conformations and assemblies in solution, *Q Rev Biophys 40*, 191-285.
55. Shvadchak, V. V., and Subramaniam, V. (2014) A four-amino acid linker between repeats in the alpha-synuclein sequence is important for fibril formation, *Biochemistry 53*, 279-281.
56. Outeiro, T. F., Putcha, P., Tetzlaff, J. E., Spoelgen, R., Koker, M., Carvalho, F., Hyman, B. T., and McLean, P. J. (2008) Formation of toxic oligomeric alpha-synuclein species in living cells, *PLoS One 3*, e1867.
57. van Rooijen, B. D., van Leijenhorst-Groener, K. A., Claessens, M. M., and Subramaniam, V. (2009) Tryptophan fluorescence reveals structural features of alpha-synuclein oligomers, *J. Mol. Biol. 394*, 826-833.

TABLES.

Table 1: Binding constants of αS monomers to SUVs

Lipid	WT K_d (μM)	H50Q K_d (μM)	G51D K_d (μM)
DOPG	54±38	24±6	32±23
CL:POPE:POPC	199±79	860±391	368±71

K_d binding constant

Table 2: Summary of the parameters obtained from SAXS data by analysis of the Guinier plot

oligomers	Guinier plot R_g, nm	$I(0)$, cm^{-1}	$N_{m/1oli}$
WT	8.8±0.3	0.68±0.04	29±4
A30P	8.3±0.1	0.35±0.04	27±5
E46K	8.9±0.4	0.66±0.29	26±7
H50Q	9.1±0.2	0.63±0.09	24±4
G51D*	7.9	0.20	31
A53T	8.8±0.4	0.66±0.2	28±1

R_g radius of gyration

$N_{m/1oli}$ number of monomers per oligomer

The errors are the standard deviation of the R_g's determined for three independently prepared batches of oligomers of the different proteins; for G51D only one batch of oligomers could be measured.

FIGURE LEGENDS

Figure 1: **Titration of αS monomers by SUVs consisting of: A) DOPG and B) CL:POPE:POPC (4:3:5).** Conformational changes of WT, H50Q and G51D aS were followed by CD spectroscopy. The membrane bound α-helical conformation is characterized by a negative peak at 222 nm in the CD spectrum. The binding affinity was determined from the changes in mean residue ellipticity (MRE) at 222 nm as a function of the lipid concentration. For determination of K_d the data were normalized to 1. Experiments were performed at 25 °C for 4 μM protein in 10 mM K-phosphate buffer, pH 7.4.

Figure 2: **Aggregation of disease-related αS mutants.** Fibril formation was followed using a classical ThT assay. **(A)** Lag times were extracted from the six individual aggregation repeats for each variant and are presented as a box plot. **(B)** The presence of fibrils in the plateau phase of aggregation is confirmed using AFM.

Figure 3: Calcein release from **(A)** DOPG and **(B)** CL:POPE:POPC LUVs as a function of the concentration of oligomeric WT (black circles) and disease-related αS mutants: A30P (red), E46K (blue), A53T (light green), H50Q (dark green) and G51D (light purple circles). The oligomer concentration is given in equivalent monomer concentration.

Figure 4: **Small-angle X-ray scattering curves of αS oligomers. (A)** Experimentally obtained SAXS curves for WT, A30P, E46K, H50Q, G51D and A53T αS oligomers. Intensity of the

buffer was subtracted from the intensity of the samples. **(B)** Averaged Guinier plots for all oligomers. From top to bottom, WT (black empty squares), A53T (black full triangles), E46K (black empty diamonds), H50Q (grey full diamonds), A30P (grey empty squares) and G51D (black full circles). **(C)** From the Guinier plots the R_g and $I(0)$ are obtained and used to calculate the M_w and number of monomers in the oligomers**.** For each protein, three independently-prepared batches of oligomers were measured, except for G51D oligomers, where we only succeeded in preparing one batch with sufficient material.

Figure 5: **Kratky plots for oligomers composed of WT and disease-related αS mutants**. **(A)** WT, **(B)** A30P, **(C)** E46K, **(D)** H50Q, **(E)** G51D and **(F)** A53T. The shape of the spectra indicates that all αS oligomers are partially folded.

FIGURES

Figure 1

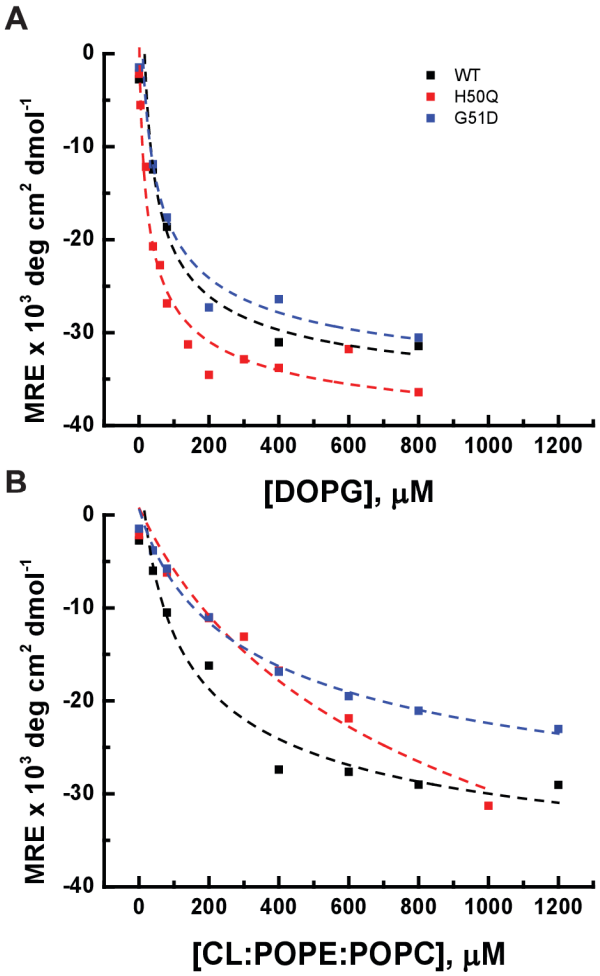

Figure 2

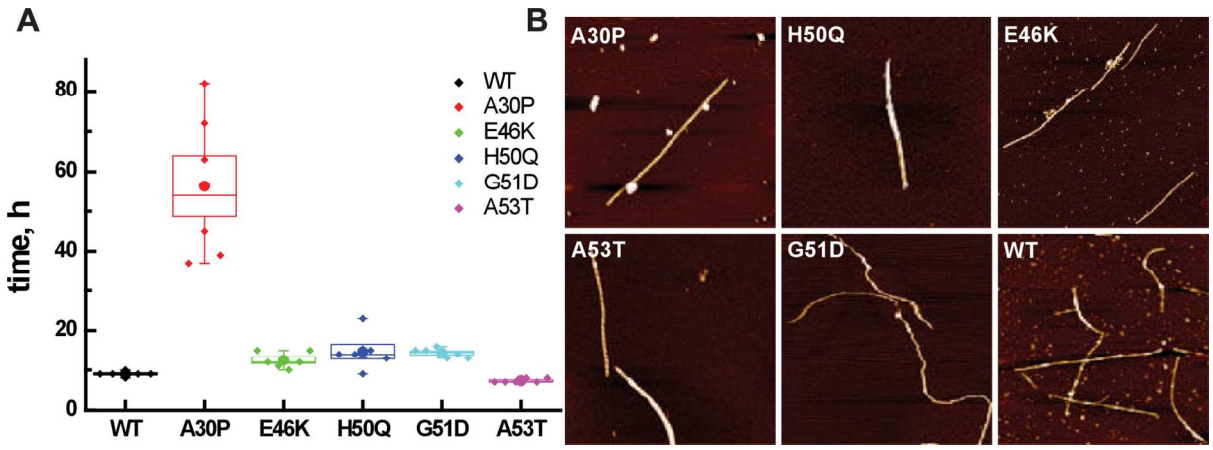
A
B
time, h
0
20
40
60
80
WT
A30P
E46K
H50Q
G51D
A53T
WT
A30P
E46K
H50Q
G51D
A53T
A30P
H50Q
E46K
A53T
G51D
WT

Figure 3

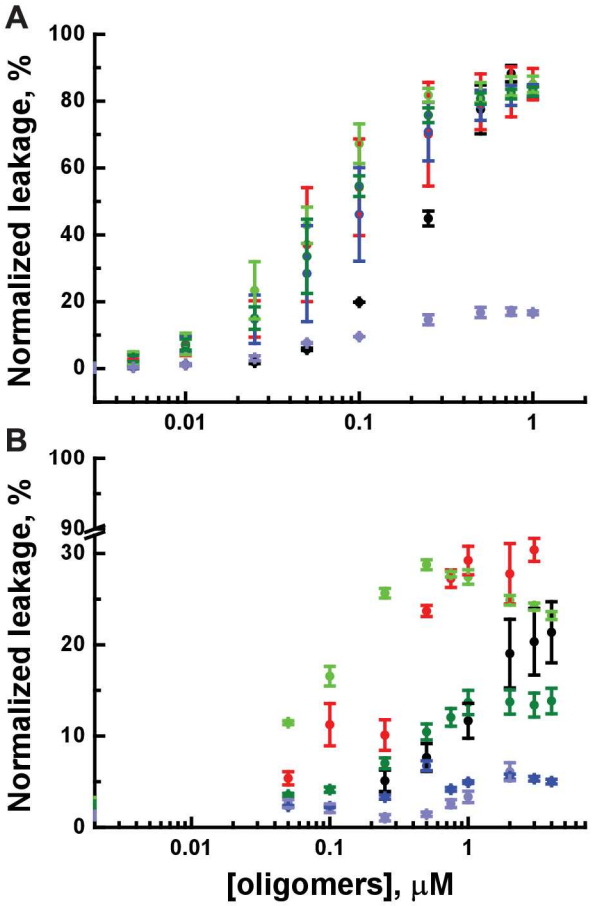
A
Normalized leakage, %
100
80
60
40
20
0
0.01
0.1
1
B
Normalized leakage, %
100
90
30
20
10
0
0.01
0.1
1
[oligomers], μM

Figure 4

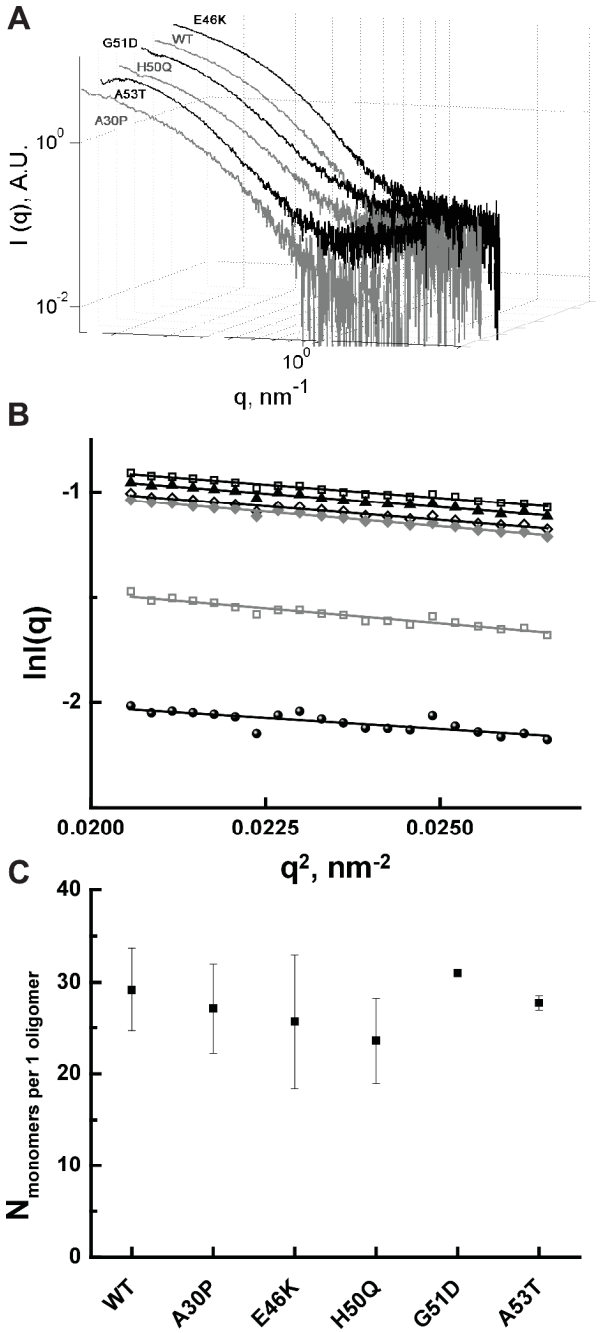
A
E46K
WT
G51D
H50Q
A53T
A30P
I (q), A.U.
10^0
10^{-2}
10^0
q, nm^{-1}
B
-1
-2
lnI(q)
0.0200
0.0225
0.0250
q^2, nm^{-2}
C
40
30
20
10
0
N monomers per 1 oligomer
WT
A30P
E46K
H50Q
G51D
A53T

Figure 5

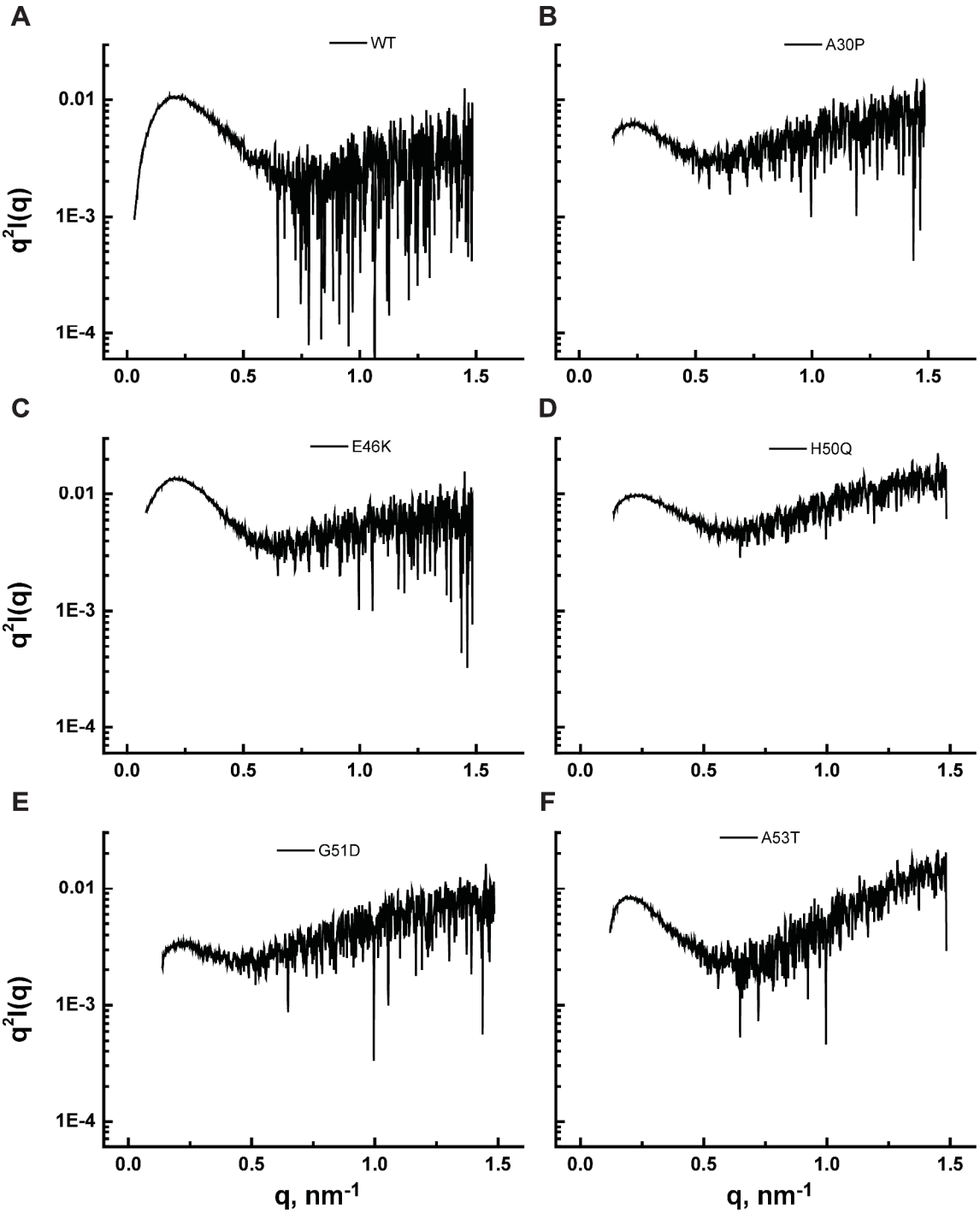
A
WT
B
A30P
C
E46K
D
H50Q
E
G51D
F
A53T
0.01
1E-3
1E-4
$q^2I(q)$
0.0
0.5
1.0
1.5
q, nm^{-1}

Table of Contents Graphic

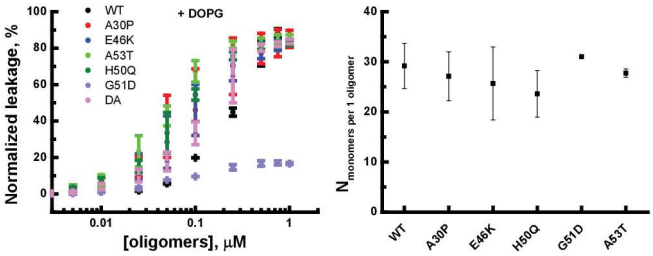

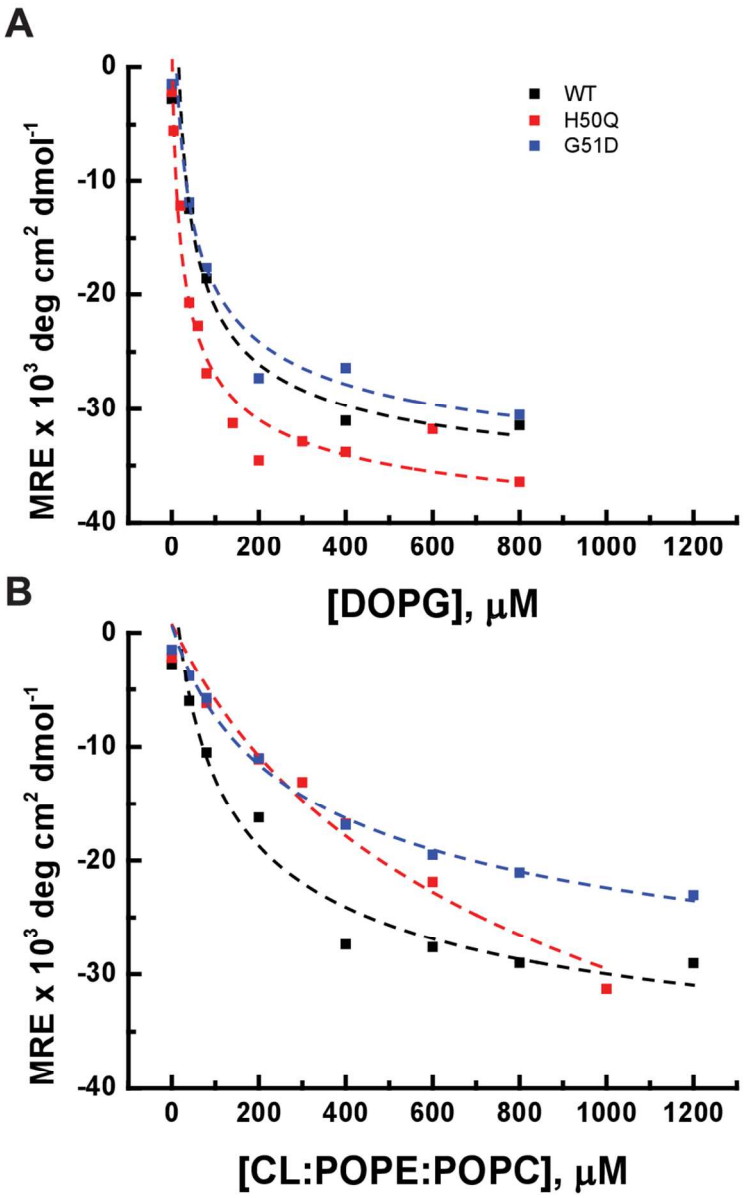

Figure 1: Titration of αS monomers by SUVs consisting of: A) DOPG and B) CL:POPE:POPC (4:3:5). Conformational changes of WT, H50Q and G51D aS were followed by CD spectroscopy. The membrane bound α-helical conformation is characterized by a negative peak at 222 nm in the CD spectrum. The binding affinity was determined from the changes in mean residue ellipticity (MRE) at 222 nm as a function of the lipid concentration. For determination of the data were normalized to 1. Experiments were performed at 25 °C for 4 µM protein in 10 mM K-phosphate buffer, pH 7.4.
80x128mm (300 x 300 DPI)

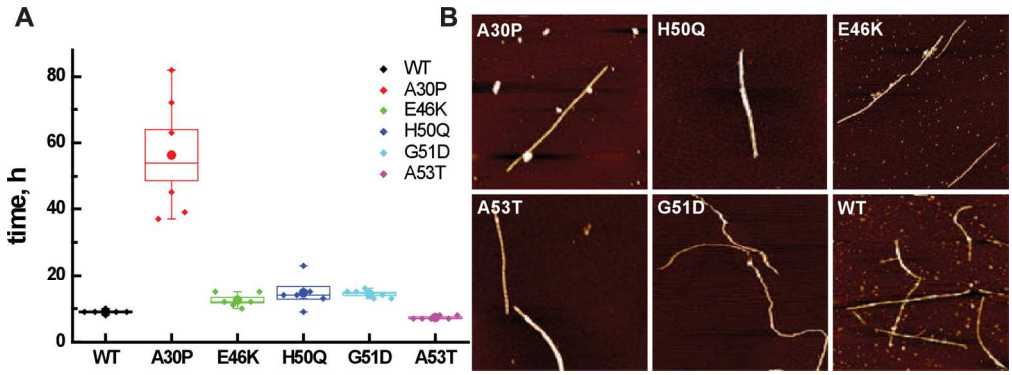

Figure 2: Aggregation of disease-related αS mutants. Fibril formation was followed using a classical ThT assay. (A) Lag times were extracted from the six individual aggregation repeats for each variant and are presented as a box plot. (B) The presence of fibrils in the plateau phase of aggregation is confirmed using AFM.
158x57mm (300 x 300 DPI)

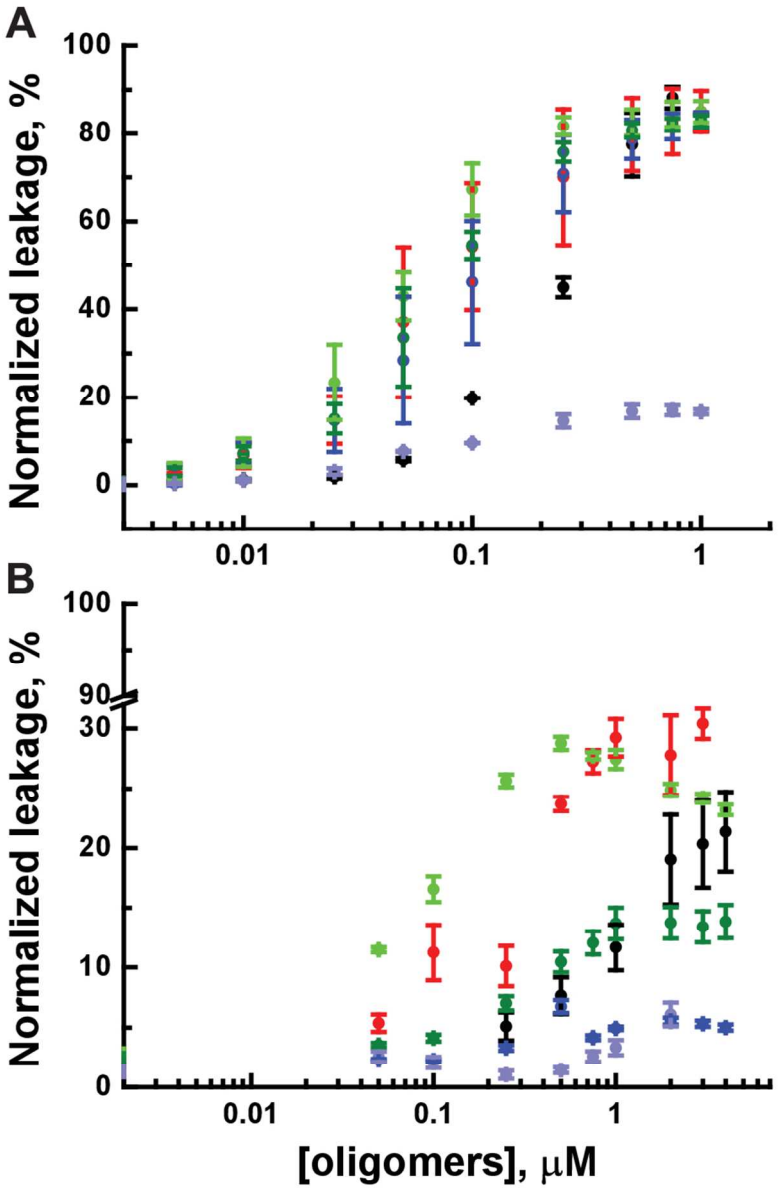

Figure 3: Calcein release from (A) DOPG and (B) CL:POPE:POPC LUVs as a function of the concentration of oligomeric WT (black circles) and disease-related αS mutants: A30P (red), E46K (blue), A53T (light green), H50Q (dark green) and G51D (light purple circles). The oligomer concentration is given in equivalent monomer concentration.
79x120mm (300 x 300 DPI)

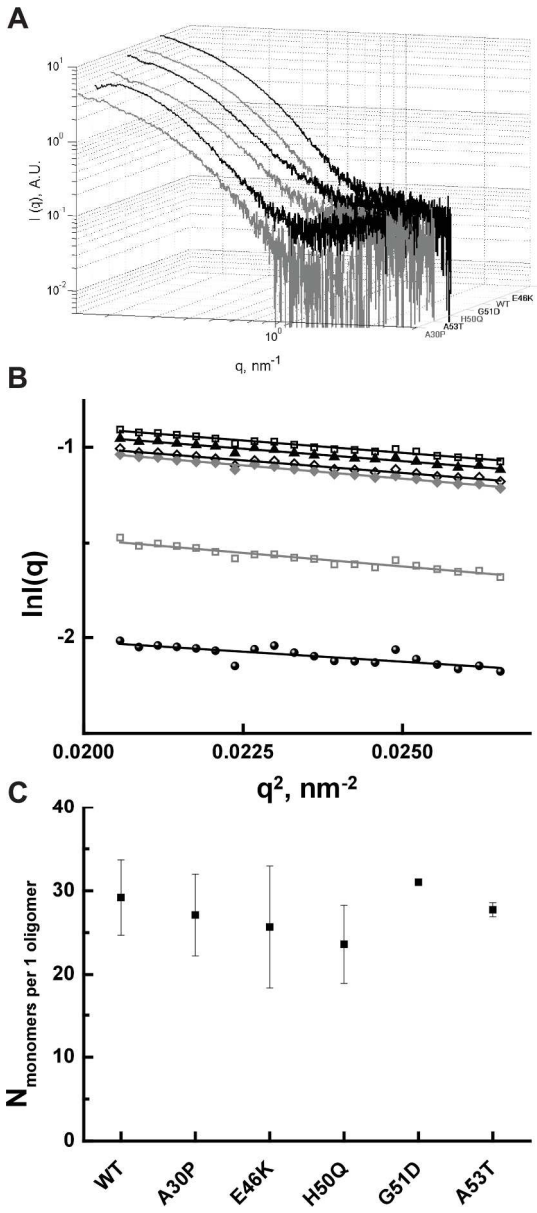

Figure 4: Small-angle X-ray scattering curves of αS oligomers. (A) Experimentally obtained SAXS curves for WT, A30P, E46K, H50Q, G51D and A53T αS oligomers. Intensity of the buffer was subtracted from the intensity of the samples. (B) Averaged Guinier plots for all oligomers. From top to bottom, WT (black empty squares), A53T (black full triangles), E46K (black empty diamonds), H50Q (grey full diamonds), A30P (grey empty squares) and G51D (black full circles). (C) From the Guinier plots the and are obtained and used to calculate the and number of monomers in the oligomers.
174x393mm (300 x 300 DPI)

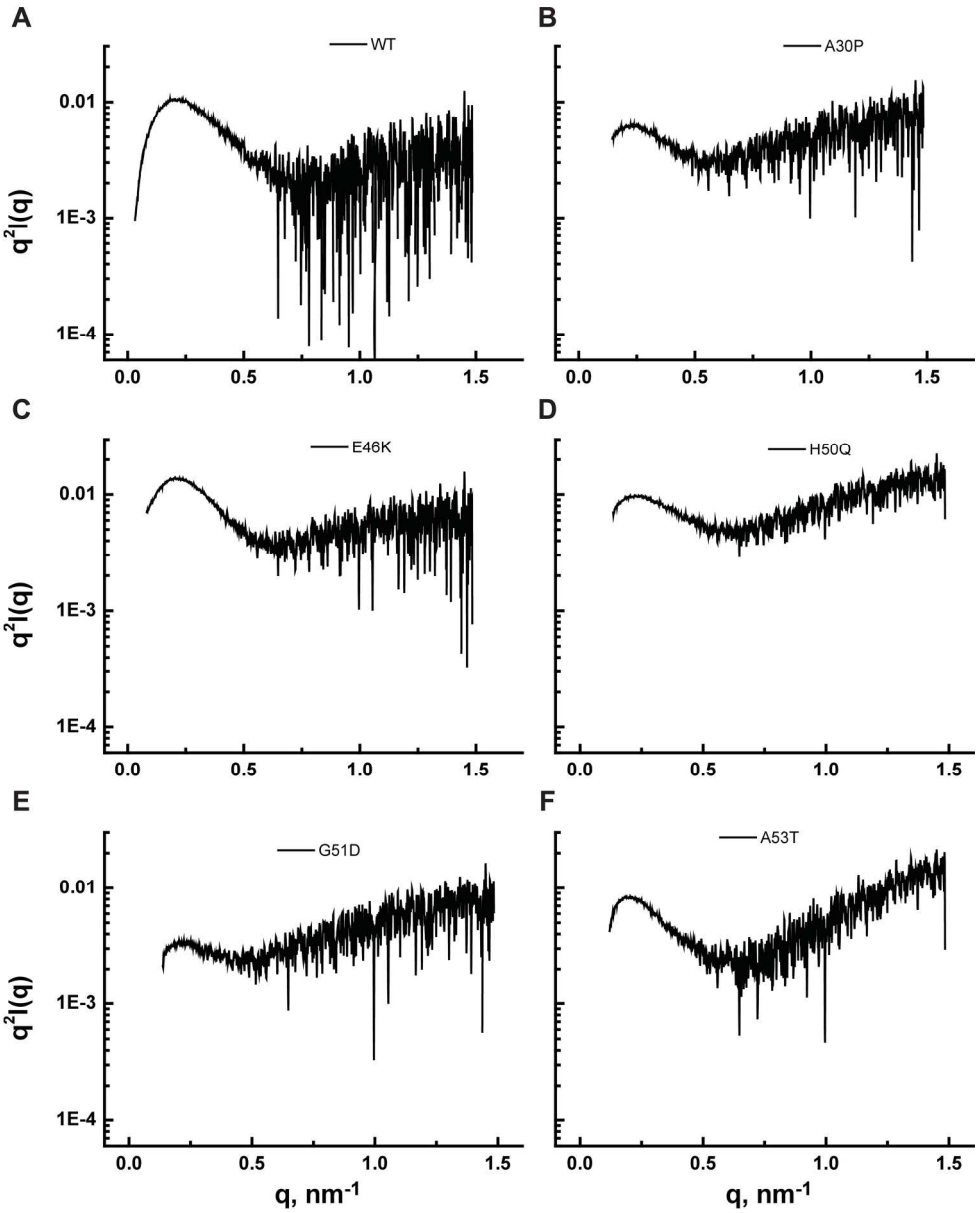

Figure 5: Kratky plots for oligomers composed of WT and disease-related αS mutants. (A) WT, (B) A30P, (C) E46K, (D) H50Q, (E) G51D and (F) A53T. The shape of the spectra indicates that all αS oligomers are partially folded.
186x229mm (300 x 300 DPI)

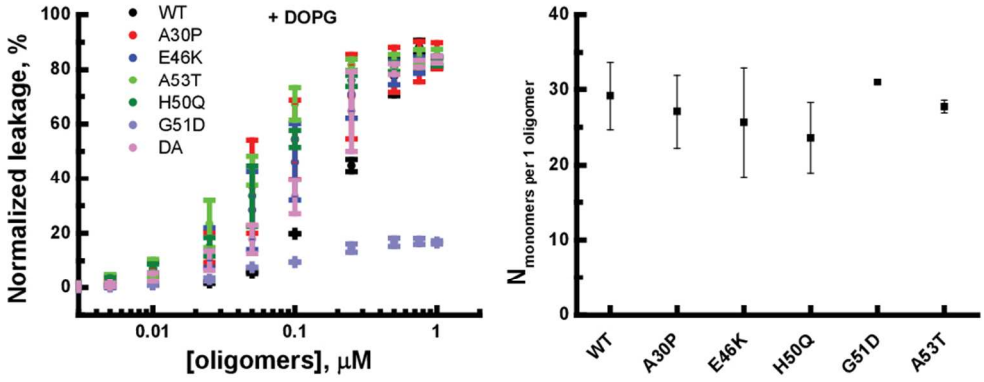

Table of Content Graphic
87x34mm (300 x 300 DPI)